THESIS

CHARACTERIZATION OF RADIATION RESPONSE FOR FIRST RESPONDER INSTRUMENTATION

Submitted by

Ryan Fabian

Department of Environmental and Radiological Health Sciences

In partial fulfillment of the requirements

For the Degree of Master of Science

Colorado State University

Fort Collins, Colorado

Summer 2019

Master's Committee:

Advisor: Alexander Brandl

Tom Johnson
Robert Gudmestad

ABSTRACT

CHARACTERIZATION OF RADIATION RESPONSE FOR FIRST RESPONDER INSTRUMENTATION

Radiation exposures of first responders can present health concerns. Some situations where such radiation exposures of first responders may exist include emergencies at nuclear power plants or facilities that house nuclear materials, coming into contact with lost or stolen nuclear material or nuclear weapons, and a dirty bomb or nuclear weapon detonation. As a result, it is important for first responders to be outfitted with equipment appropriate for each of these emergency situations. One such piece of equipment is an electronic personal dosimeter (EPD). EPDs are capable of providing real-time dose and dose rate data, and can also produce audible alarms triggered when preset dose rate levels are exceeded; however, electronic personal dosimeters do not discriminate natural background radiation contributing to their signal. This can result in the first responders becoming distracted/confused by dose or dose rate readouts from natural background radiation, or in missed real radiation exposure threats from unknown sources. An algorithm which would allow for the discrimination of natural background radiation from an EPD's signal was developed in the course of this project. If applied and implemented in a commercial EPD, this algorithm will allow first responders to distinguish directly between a readout due to naturally occurring radon progeny in the environment and contributions from other sources of ionizing radiation.

ACKOWLEDGEMENTS

I would like to express my gratitude to my advisor Dr. Alexander Brandl for the direction and mentorship that he provided throughout my time at Colorado State University. I would also like to thank Dr. Thomas Johnson, Dr. Ralf Sudowe, and Dr. Tom Borak for providing valuable knowledge and support while here at Colorado State University. To my fellow classmates, thank you for your support, encouragement, and friendship. Finally, I would like to thank my wife Brandie for supporting me throughout my educational journey, and my children for sacrificing much during this period. Thank you.

TABLE OF CONTENTS

LIST OF TABLES

LIST OF FIGURES

CHAPTER 1 INTRODUCTION

Radiation exposures of first responders can present health concerns. Some situations where such radiation exposures of first responders may exist include emergencies at nuclear power plants or facilities that house nuclear materials, coming into contact with lost or stolen nuclear material or nuclear weapons, and a dirty bomb or nuclear weapon detonation. As a result, it is important for first responders to be outfitted with equipment appropriate for each of these emergency situations. One such piece of equipment is an electronic personal dosimeter (EPD). EPDs are capable of providing real-time dose and dose rate data, and can also produce audible alarms triggered when preset dose rate levels are exceeded; as a result, EPDs are well suited for use by first responders. Due to possible health effects as a result of excess exposure to radiation, it is important that a first responder's EPD works properly if they find themselves in a situation where a potential for radiation exposure exists. The radiation response for an EPD being considered for use by first responders was investigated, and the feasibility of using the data from the EPD to determine the gamma dose or dose rate contributed by radon and its daughter products is explored.

Certain electronic personal dosimeters utilize solid state detector technology and complex algorithms to provide real time dose and dose rate readouts to users. The ability to provide real time readouts makes EPDs a valuable tool for individual monitoring in radiation protection. In order to provide real time dose and dose rate readouts, the generic operations of an EPD utilizing solid state detectors are:

1. Ionizing radiation interacts with a solid state detection material, such as silicon, and deposits some or all of its energy within the material.

2. This energy deposition strips an electron from an atom within the material. The remaining ion is referred to as a hole.
3. An electric field is applied to the material which causes the electron and hole to migrate in opposite directions, and subsequently, be collected on an anode and cathode, which creates a current within a circuit (Knoll, 2010).
4. Electronics within the detector then amplify and shape the current into a digital signal.
5. An algorithm then converts the data obtained from the digital signal to determine the dose and dose rate.

Though this process produces real time readouts, not all of the energy from the ionizing radiation is deposited within the detector, which produces a current that is not directly proportional to the dose. Instead, the algorithm within the detector utilizes a calibration factor to convert the signal to a dose. This is a result of size limitations of EPDs. Current technological capabilities limit the size and thickness of solid state detectors, such that the active region of the detector material is small. It is for this reason, that silicon is utilized in these detectors. Silicon is highly sensitive to interactions with ionizing radiation, which allows for the detection of a wide range of radiation types and energies over a small detection volume (Omar, 2010).

While multiple design types exist for EPDs, a two-silicon diode configuration was modeled in Monte Carlo N-Particle (MCNP) simulations (Los Alamos National Laboratory, Los Alamos, New Mexico). The two-silicon diode configuration was chosen for the purpose of discrimination of the photon contribution from the Rn-222 progeny. Having two-silicon diodes, allows for the comparison of signals between the two, and an easier derivation of an equation needed to calculate the gamma radiation contribution. One filtered silicon diode was used to

model the detector response to gamma radiation, and one unfiltered silicon diode was used to model the detector response to beta particles. In addition to this, MCNP modeling was utilized to determine the radiation response of this configuration to Rn-222 and its progeny. Specifically, MCNP modeling was utilized to determine the theoretical values of the ratio of Rn-222 progeny beta interactions on the unfiltered diode versus the Rn-222 progeny gamma interactions on the filtered diode ($K_{\beta/\gamma}$), and the ratio of beta interactions on the unfiltered diode versus beta interactions on the filtered diode (K_{β}) for the Rn-222 progeny. Utilizing these data, an algorithmic process to subtract the gamma ray contributions from Rn-222 and its progeny in EPDs was derived.

Cs-137 is a non-naturally occurring radionuclide with a half-life of 30.17 years. It can be produced via nuclear fission processes of U-235 in nuclear reactors. Cs-137 decays via two methods. The first emission process occurs through the emission of a β^- particle with a maximum energy of 512 keV. This transition occurs in 94.7% of all Cs-137 transitions and results in the creation of a Ba-137 nucleus in a metastable state (Ba-137m). The resulting Ba-137m nucleus is left in an excited state, which then decays further by emitting a 662 keV gamma ray in 89.9% of all Ba-137m transitions. The result of this transition is a stable Ba-137 nucleus. The second Cs-137 decay process involves the emission of a β^- particle of a maximum energy of 1174 keV in 5.3% of the Cs-137 transitions, which directly produces the stable Ba-137 nucleus. As a result of these processes, a 662 keV gamma ray is released in 85.1% of all Cs-137 transitions (Johnson, 2017). A Cs-137 decay scheme can be found in Figure 1.

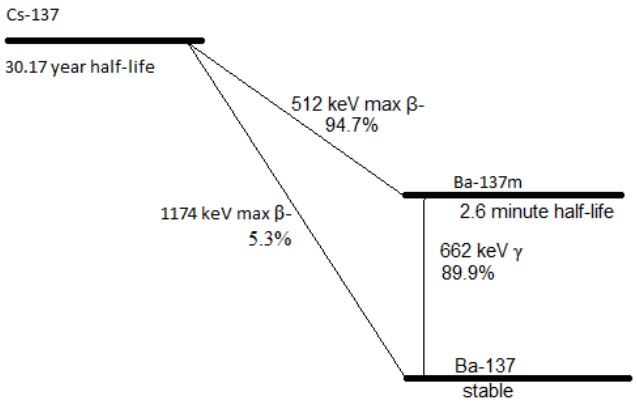

Figure 1. Cs-137 decay scheme

For this project, only the 662 keV gamma ray produced by the Cs-137 decay chain is of interest.

Gamma rays largely interact with matter via three main processes: photoelectric absorption, Compton scattering, and pair production. Photoelectric absorption is governed by the photoelectric effect. In this process, a gamma ray transfers all of its energy to a tightly bound electron of an atom. The difference in energy between the incident photon and the free electron is equal to the binding energy of the electron. The resulting free electron from this interaction is a primary ionizing particle, which is commonly known as a photoelectron. The photoelectron energy can be calculated via the following equation (Johnson, 2017):

$$E_{photoelectron} = hf - \varphi, \quad (1)$$

where h is the Planck constant, f is the frequency of the gamma ray, and φ is the tightly bound electron's binding energy. Gamma rays of low energies have a greater probability of interacting with matter via the photoelectric effect. Compton scattering occurs when an incident photon is deflected by an electron. In this interaction, the photon can impart a portion of its energy to the electron. The angle θ by which the photon is scattered is directly related to the total energy

transferred to the electron and the energy associated with the scattered photon. The energies associated with the scattered photon ($E_{\gamma f}$), and the scattered electron (E_{ef}) are given by the following (Johnson, 2017):

$$\mathrm{E_{\gamma f}} = \frac{1}{1+\frac{\mathrm{E_{\gamma i}}}{0.511\mathrm{MeV}}(1-\cos\theta)}, \tag{2}$$

$$\mathrm{E_{ef}} = \frac{\frac{\mathrm{E_{\gamma i}}}{0.511\mathrm{MeV}}(1-\cos\theta)}{1+\frac{\mathrm{E_{\gamma i}}}{0.511\mathrm{MeV}}(1-\cos\theta)}, \tag{3}$$

where $\mathrm{E_{\gamma i}}$ is the energy of the incident photon, and $0.511\mathrm{MeV}$ is the rest mass energy of an electron. Of these interactions, Compton scattering is the most probable for the gamma ray energies associated with Cs-137; however, it is possible for photoelectric absorption to occur. Pair production occurs when a photon with energy greater than or equal to 1.022 MeV spontaneously converts 1.022 MeV of its energy into mass, while passing near a nucleus. The 1.022 MeV energy is converted into an electron-positron pair; however, pair production is neglected here, as the minimum photon energy associated with this process is 1.022 MeV, which is much larger than the 662 keV gamma ray emission from Cs-137.

The EPD being investigated provides users with real time dose and dose rate measurements. As a result, the radiation detection devices chosen to calibrate this source needed to be capable of accurately measuring dose and dose rate. Since tissue equivalent ion chambers are capable of dose and dose rate measurements, a tissue equivalent ion chamber was chosen for this project (American Association of Physicists in Medicine, 2012).

Ionization chambers are gas filled chambers that utilize the effects caused by interactions of charged particles with a gas. In ionization chambers, ionizing radiation can ionize gas molecules and create electron/ion pairs, which consist of an electron and a positively charged

ion. The electron/ion pairs are then accelerated via an electric field that is large enough to keep recombination of electrons and positively charged ions from occurring and small enough so that the electron/ion pairs cannot produce further ionizations. The electron is subsequently collected by an anode, and the positively charged ion is collected by a cathode. The collection of these electron/ion pairs produces a current, which is directly proportional to the amount of energy that is deposited within the fill gas that is contained within the ionization chamber (Johnson, 2017); however, the current that is typically created is so small that it is difficult to detect. Instead, ion chambers can be designed to detect a change in voltage caused by the induced current, as voltage and current are directly related via the following relationship (Knight & Jones, 2010):

$$V = IR, \tag{4}$$

where V is the voltage, I is the current, and R is the resistance in the circuit. Using this equation, the change in voltage can be directly related to the change in current (Knight & Jones, 2010):

$$\Delta V = \Delta I \times R, \tag{5}$$

where ΔV is the change in voltage, and ΔI is the change in current. While this relationship between voltage and current is relatively straight forward, consistent measurement using circuitry is a bit more complicated. Given this, the voltage in ionization chambers is commonly measured using a RC circuit, given the following relationship (Johnson, 2017):

$$V(t) = V_{ss}(1 - e^{-\frac{t}{RC}}), \tag{6}$$

where V(t) is the voltage at time t, V_{ss} is the steady state voltage, R is the total resistance of the circuit, and C is the total capacitance of the circuit.

Tissue equivalent ionization chambers are capable of directly measuring dose and dose rates. Tissue equivalent ionization chambers have pressurized chambers with chamber walls that are constructed with tissue equivalent materials. Tissue equivalent materials have similar gamma ray and charged particle interaction characteristics as soft tissue. When gamma rays interact with the tissue equivalent material, they can interact via photoelectric absorption, Compton scattering, or pair production. These interactions create a primary ionizing electron, which can then deposit energy within the fill gas of the ionization chamber. This process is explained by the Bragg-Gray principle, which states that the energy deposited into a tissue equivalent material surrounding the fill gas in an ionization chamber is proportional to the ionization produced in the fill gas within the chamber; however, in order for this direct proportionality to be accurate, electronic equilibrium at the tissue equivalent material must be established. If electronic equilibrium is established, the energy absorbed for a given mass unit of tissue equivalent material is directly associated to the energy absorbed for a given mass unit of fill gas in the ionization chamber via the following relationship (Johnson, 2017):

$$\frac{dE_{TE}}{dM_{TE}} = \frac{S_{TE}}{S_{gas}} \times \omega \times J\,, \tag{7}$$

where S_{TE} is the mass stopping power of the tissue equivalent material, S_{gas} is the mass stopping power of the fill gas in the ionization chamber, ω is the average energy required to produce an electron/ion pair in the fill gas, and J is the total number of electron/ion pairs for each unit mass of gas.

In order to properly calibrate a radiation detection device, the National Council on Radiation Protection and Measurements' (NCRP) NCRP Report No. 112 recommends the use of a calibrated source that is National Institute of Science and Technology (NIST) traceable

(National Council on Radiation Protection and Measurements, 1991). To accomplish the source calibration, guidance provided in NCRP Report No. 112 was followed, and a NIST calibrated instrument was used (National Council on Radiation Protection and Measurements, 1991). The NIST calibrated instrument used for this project is a Ludlum 9DP ion chamber calibrated by NIST in December of 2018 (Ludlum Measurements, INC., Sweetwater, Texas). The NIST calibration conducted is listed as code 46010C, which is a gamma ray calibration that was conducted at an air kerma rate ($\dot{K}$) of $\dot{K} = 9.0 \times 10^{-7} \mathrm{Gy/s}$.

The Ludlum 9DP ion chamber is a tissue equivalent ion chamber and is filled with a mixture of 99.89% nitrogen gas and 0.11% argon gas, which are pressurized to 9 atm (Ludlum Measurements, INC., 2018). Nitrogen gas has a first ionization potential of 15.5 eV, and argon gas has a first ionization potential of 15.7 eV (Knoll, 2010). These first ionization potentials make the Ludlum 9DP ion chamber an ideal detector for use with Cs-137 sources (Johnson, 2017).

For verifying the calibration results obtained with the NIST calibrated Ludlum 9DP ion chamber, MCNP simulations were conducted. MCNP is a known benchmarking software that is utilized for instrumentation testing (Los Alamos National Labratory, 2018). Utilizing MCNP, simulations can be run to determine an expected photon fluence for a modeled scenario at a given point. Then, dose rates can be extrapolated from these data, and used as a standard for the given scenario.

The Cs-137 source within the JL Shepard Model 28-8b produces an isotropic radiation field; however, the majority of the radiation field generated is shielded and collimated by the lead housing of the irradiator. As a result, only a small part of the radiation field is emitted as a beam from a small hole in the front of the irradiator. The intensity of the collimated beam should

closely follow the inverse square law, as the Cs-137 source emits radiation isotopically and few scattering events are expected to take place within the room housing the irradiator. Therefore, the intensity of the beam can be calculated by the following (Knight & Jones, 2010):

$$I(r) = \frac{I_0}{r^2}, \tag{8}$$

where $I(r)$ is the intensity of the beam at a distance r from the source, and I_0 is the intensity of the beam at a reference location at a given distance from the source.

Furthermore, to calibrate the JL Shepard Model 28-8B irradiator, multiple measurements were taken at various distances along the center line of the irradiator. Given the assumption that the intensity of the beam follows the inverse square law, the data acquired via these measurements were used to obtain a fitted dose rate equation, which can be used to determine the expected dose rate at any position along the center line of the irradiator.

The radiation response to Rn-222 and its progeny was investigated, as radon is the largest contributor to natural background radiation. Through understanding the radiation response to the Rn-222 progeny, it is possible to approximate their contribution to the total dose measured by the EPD via a calculation. This could then be used to discriminate the radon and progeny contribution to the dose or dose rate readout; however, these calculations assume that Rn-222 and its progeny are the only source contributing to the beta interactions in the detector. Being that beta particles are easily shielded and have a relatively short range in air, this assumption should hold in the majority of circumstances.

CHAPTER 2 MATERIALS AND METHODS

The following tasks were completed to determine the radiation response of an EPD to gamma radiation and the theoretical radiation response of an EPD to the Rn-222 progeny. The tasks are separated into three categories:

1. The calibration and characterization of the Cs-137 Source in MRB.
2. Physical testing of the EPD utilizing the Cs-137 source in MRB.
3. MCNP modeling to determine the theoretical EPD radiation response to the Rn-222 progeny.

In order to investigate the EPD radiation response to gamma radiation, a calibrated source was used for physical testing. A JL Shepard Model 28-8B irradiator housing a Cs-137 source in the Molecular and Radiological Biosciences building (MRB) which is used by Colorado State University's Radiation Control Office (RCO) for radiation detection device calibration was chosen for all physical EPD testing. The JL Shepard Model 28-8B irradiator in MRB was recalibrated for this project. The calibration was completed by using a NIST calibrated Ludlum 9DP ion chamber, and MCNP. Utilizing the Ludlum 9DP, ten 30 second measurements were taken at nine positions located at 0.5 m, 0.75 m, 1 m, 1.25 m, 1.5 m, 2 m, 2.5 m, and 3 m from the source along the beam center line. Distances from the source were measured using a measuring tape and an indicator was placed along the center line for each of the distances listed. The Ludlum 9DP was then oriented perpendicularly to the center line of the Cs-137 beam and placed so that the active volume was centered on the distance/center line indicator for that distance. The instrument was active for thirty second during each exposure, but the dose rate read out on the Ludlum 9DP was recorded at the 15 second mark of each exposure. The

integrated dose readout was recorded at the conclusion of the full measurement interval. A minimum of thirty seconds was allowed to elapse between each subsequent measurement, so that no issues of saturation could potentially arise. The dose rate measurements recorded were then manipulated utilizing the following function to produce an average dose rate in the units of mSv/h for each position:

$$\dot{\bar{D}}(x) = \frac{\sum_{i=1}^{10} Y_i \cdot 1.037}{10}, \tag{9}$$

where, Y_i (mSv/h) is the ith measurement at the distance x from the source, and 1.037 is the calibration factor provided by NIST following the calibration of the Ludlum 9DP. A sample file including dose rate measurements and subsequent manipulations can be found in Table 1.

Table 1. Sample Ludlum 9DP measurements and data manipulation

Distance (m)	Measurement 1	Measurement 2	Measurement 3	Measurement 4	Measurement 5	Measurement 6	Measurement 7	Measurement 8	Measurement 9	Measurement 10
0.5	7.64	7.65	7.68	7.69	7.68	7.70	7.69	7.71	7.68	7.68
0.75	3.53	3.51	3.52	3.53	3.52	3.54	3.51	3.53	3.52	3.51
1	1.96	1.97	1.96	1.96	1.97	1.96	1.97	1.96	1.96	1.96
1.25	1.26	1.27	1.29	1.27	1.26	1.26	1.26	1.27	1.27	1.27
1.5	0.88	0.89	0.88	0.88	0.89	0.88	0.88	0.88	0.88	0.88
1.75	0.66	0.66	0.65	0.66	0.67	0.66	0.66	0.66	0.66	0.66
2	0.50	0.50	0.50	0.50	0.51	0.51	0.51	0.50	0.50	0.51
2.5	0.33	0.33	0.33	0.33	0.33	0.33	0.33	0.33	0.33	0.34
3	0.23	0.23	0.22	0.22	0.22	0.22	0.22	0.22	0.23	0.23

In order to compare these results, MCNP modeling of the MRB Cs-137 source facility was conducted. Utilizing MCNP, the room housing the source was modeled. The walls, ceiling, table and JL Shepard Model 28-8b irradiator were all modeled, while the lights, electrical conduits, and other small items were omitted from the model. It was determined by the investigator that the omitted items would not contribute to the validity of the model, as very few scattering events would be directed back towards the measurements positions. The Cs-137 source was modeled as a point source at the center of a cavity within the JL Shepard Model 28-8b irradiator housing. Nine F5 tally locations were placed at the same measurement positions that were utilized for the Ludlum 9DP measurements. Each tally includes a photon fluence to

dose conversion factor obtained from ICRP 119 that converts the F5 tally output of photon fluence to a unit in Gy/photon (ICRP, 2012). The original ICRP 119 conversion factor produces a unit of μGy/photon; however, this was modified to produce the final unit of Gy/photon for this project. The model was then run simulating 200,000,000 particles. The tally outputs were then further manipulated to a dose rate in units of mSv/h by the following:

$$\dot{\mathrm{D}}(\mathrm{x})_{MCNP} = \mathrm{Y}(\mathrm{x}) \cdot \mathrm{A}_{Source} \cdot \rho \cdot 3600 \frac{\mathrm{s}}{\mathrm{h}} \cdot 10^3 \frac{mSv}{Gy}, \tag{10}$$

where $\mathrm{Y}(\mathrm{x})$ is the MCNP F5 tally output at a distance x from the source, A_{Source} is the activity of the MRB Cs-137 source [Bq] at the time of the Ludlum 9DP measurements, and ρ is the probability that a Cs-137 decay will produce a 662 keV photon. A sample file including measurements and subsequent manipulations can be found in Table 2.

Table 2. Sample MCNP MRB Cs-137 data and manipulations

Distance (m)	Gy/photon	Source Activity (Bq)	Photon per Disintegration	Dose Rate (Gy/s)	Dose Rate (Gy/h)	Dose Rate (mSv/h)
0.5	1.09E-16	23322987000	0.85	2.17E-06	7.80E-03	**7.80**
0.75	4.99E-17	23322987000	0.85	9.90E-07	3.56E-03	**3.56**
1	2.89E-17	23322987000	0.85	5.73E-07	2.06E-03	**2.06**
1.25	1.90E-17	23322987000	0.85	3.76E-07	1.35E-03	**1.35**
1.5	1.34E-17	23322987000	0.85	2.66E-07	9.59E-04	**0.96**
1.75	1.00E-17	23322987000	0.85	1.98E-07	7.14E-04	**0.71**
2	7.74E-18	23322987000	0.85	1.54E-07	5.53E-04	**0.55**
2.5	5.05E-18	23322987000	0.85	1.00E-07	3.60E-04	**0.36**
3	3.57E-18	23322987000	0.85	7.08E-08	2.55E-04	**0.25**

The results from the MCNP modeling and the Ludlum 9DP measurements were compared to ensure proper characterization of the MRB Cs-137 source. A two-sample t-test was conducted for this comparison.

A two-sample t-test can be used to determine whether or not two means are equal provided a pre-determined statistical confidence level. The test statistic was calculated via the following (NIST, 2019):

$$t = \frac{\bar{x}_1 - \bar{x}_2}{\sqrt{\frac{s_1^2}{n_1} + \frac{s_2^2}{n_2}}}, \tag{11}$$

where $\bar{x}_1$ is the first mean (MCNP mean), $\bar{x}_2$ is the second mean (mean obtained from the Ludlum 9DP measurements), s_1 is the standard deviation for mean one, s_2 is the standard deviation for mean two, n_1 is the sample size of mean one, and n_2 is the sample size of mean two. The standard deviation can be calculated via the following:

$$s = \sqrt{\frac{\sum_{i=1}^{n}(x_i - \bar{x})^2}{n}}, \tag{12}$$

where x_i is the ith sample measurement, $\bar{x}$ is the mean of sample, and n is sample size. The mean of the sample and the sample size assume the same values utilized in equation 13. Then the degrees of freedom need to be determined via the following:

$$df = \frac{\left(\frac{s_1^2}{n_1} + \frac{s_2^2}{n_2}\right)^2}{\frac{\left(\frac{s_1^2}{n_1}\right)^2}{n_1 - 1} + \frac{\left(\frac{s_2^2}{n_2}\right)^2}{n_2 - 1}} \tag{13}$$

Utilizing the degrees of freedom and the chosen significance level, a critical value can be found in a t-table. If $|t|$ is larger than the critical value found in the t-table, the means are not equal at the chosen significance level. Alternatively, if $|t|$ is smaller than the critical value found in the t-table, the means are equal at the chosen significance level.

Following the characterization of the MRB Cs-137 source, physical testing of the EPD was conducted. First, ten 30 second measurements were conducted at the same nine distances from the Cs-137 source as were used for the MCNP modeling and Ludlum 9DP measurements. At approximately the 15 second mark of the measurements, the dose rate readout on the EPD

was recorded. The ten dose rate measurements for each location were then averaged, and the averages were then compared to the results from the Ludlum 9DP measurements and the MCNP modeling. Again, a two-sample t-test was conducted for these comparisons.

Finally, MCNP modeling was conducted to determine the theoretical EPD radiation response to Rn-222 and its progeny. A theoretical two silicon diode detector with a Mylar® window was modeled in MCNP. The first diode had no filters and was utilized for beta detection. The second diode was modeled with three filter materials, which were used to flatten out the energy response to gamma radiation, as silicon diode detectors over respond to low energy gamma radiation and under respond to high energy gamma radiation (Lee, Lee, & Lee, 2003). The filter design was taken from a journal report, and consists of 0.08 mm of Ta, 0.2 mm Sn, 0.5 mm Cu, and 0.5 μm Al (Mitra, et al., 2016). The silicon diodes are 10 mm × 10 mm on the face and are 300 μm thick. The detectors were placed in air. F8 Tallies were utilized to determine the total number of particles that deposited any energy in either of the silicon diodes. A 1 m × 1 m × 1 m source sampling volume was created within air. The source card was created so that the starting particle locations of Rn-222 and its progeny used in the model would be homogenously distributed throughout the sampling volume in order to replicate a volume of air containing radon gas. Three MCNP simulations were created to model the energies and emission probabilities associated with the beta decays of Bi-214 and Pb-214, and the main gamma decays for the Rn-222 progeny. The beta decay energies and associated probabilities for Bi-214 and Pb-214 were taken from ICRP Publication 107 (ICRP, 2008). The main gamma emission energies and associated probabilities per Rn-222 decay were taken from the literature (Morel, Etcheverry, & Picolo, 1998). No, information from Rn-222 is being utilized. Instead, information from the Rn-222 progeny is used; as a result, the equilibrium factor associated with Rn-222 is not necessary.

Each of the three MCNP simulations were run utilizing 200,000,000 starting particles. The F8 tally output provides the total number of particle interactions per starting particle that occurred during the simulation in each of the two silicon diode detectors.

To ensure that alpha particle emissions from the Rn-222 progeny did not contribute to any measurements by the EPD, a MCNP simulation was conducted. The effect of a 7.69 MeV alpha particle on the silicon diode detector was modeled. This energy was chosen as it is the highest energy alpha particle emitted by the Rn-222 progeny. If an alpha particle with 7.69 MeV does not contribute to the measurements of the EPD, it can be concluded that lower energy alpha particles would not either. The range of an alpha particle is energy dependent, with higher energy alpha particles having the greatest range (Johnson, 2017). The same geometry used for the beta and gamma testing was maintained, and 200,000,000 particles were run.

Using the number of interactions modeled for each silicon diode scaled for the number of starting particles in the three MCNP simulations, the total number of interactions per Rn-222 progeny decay per silicon diode was obtained. The results from the Bi-214 simulations were corrected, as only 64.07% of all Bi-214 decays are beta decays. Following this, the total number of interactions per Rn-222 progeny decay in the filtered silicon diode was calculated by adding the number of interactions obtained in the filtered diode from each of the three runs. This provided the total number of gamma ray interactions per Rn-222 progeny starting particle in MCNP (C_f):

$$C_f = \varepsilon + \delta + \rho = \frac{\gamma \text{ interactions}}{Rn{-}222\ decay}, \tag{14}$$

where ε is the total number of interactions in the filtered diode per Bi-214 decay, δ is the total number of interactions in the filtered diode per Pb-214 decay, and ρ is the total number of interactions in the filtered diode from gamma rays per Rn-222 progeny decay. This process was repeated for the unfiltered silicon diode, providing the total number of beta interactions per Rn-222 progeny starting particle in MCNP (C_u):

$$C_u = \tau + \omega + \sigma = \frac{\beta \text{ interactions}}{Rn{-}222\ decay}, \tag{15}$$

where τ is the total number of interactions in the unfiltered diode per Bi-214 decay, ω is the total number of interactions in the unfiltered diode per Pb-214 decay, and σ is the total number of interactions in the unfiltered diode from gamma rays per Rn-222 progeny decay. Also, the gamma ray correction factor (f) was determined by the following:

$$\mathrm{f} = \frac{\rho}{\sigma} \tag{16}$$

A sample of the MCNP data and subsequent manipulations can be found in Table 3.

Table 3. Sample MCNP Rn-222 progeny data and manipulations

MCNP Two Diodes 200,000,000 particles	Bi214	Bi214 Prob. Corrected	Pb214	Gamma (Radon Spectrum)
Interactions per starting particle Filtered Diode	0.000169	0.000108	0.000126	0.000746
Interactions per starting particle Unfiltered Diode	0.000739	0.000473	0.000473	0.000777
Total Interactions Per Radon Decay Filtered Diode (θ)	0.000980			
Total Interactions Per Radon Decay Unfiltered Diode (ϕ)	0.001723			
K_β	4.040			
$K_{\gamma/\beta}$	0.821			
Gamma ray correction factor (f)	0.960			
1 m^3 source sampling volume				

CHAPTER 3 RESULTS AND DISCUSSION

Utilizing the Ludlum 9DP, calibration of the MRB Cs-137 source was completed. A total of 10 measurements at 9 distances from the Cs-137 source were taken. The raw data obtained from these measurements can be found in Table 4.

Table 4. Ludlum 9DP uncorrected measurement data for the MRB Cs-137 source

Ludlum 9DP MRB Cs-137 30-second measurements units mSv/(hr) uncorrected										
Distance (M)	Measurement 1	Measurement 2	Measurement 3	Measurement 4	Measurement 5	Measurement 6	Measurement 7	Measurement 8	Measurement 9	Measurement 10
0.5	7.64	7.65	7.68	7.69	7.68	7.70	7.69	7.71	7.68	7.68
0.75	3.53	3.51	3.52	3.53	3.52	3.54	3.51	3.53	3.52	3.51
1	1.96	1.97	1.96	1.96	1.97	1.96	1.97	1.96	1.96	1.96
1.25	1.26	1.27	1.29	1.27	1.26	1.26	1.26	1.27	1.27	1.27
1.5	0.88	0.89	0.88	0.88	0.89	0.88	0.88	0.88	0.88	0.88
1.75	0.66	0.66	0.65	0.66	0.67	0.66	0.66	0.66	0.66	0.66
2	0.50	0.50	0.50	0.50	0.51	0.51	0.51	0.50	0.50	0.51
2.5	0.33	0.33	0.33	0.33	0.33	0.33	0.33	0.33	0.33	0.34
3	0.23	0.23	0.22	0.22	0.22	0.22	0.22	0.22	0.23	0.23

The data in Table 4 were then corrected to account for the calibration factor provided by NIST. The corrected data can be found in Table 5.

Table 5. Ludlum 9DP calibration corrected measurement data for the MRB Cs-137 source

Ludlum 9DP MRB Cs-137 30-second measurements units mSv/(hr) calibration corrected												
Distance (M)	Measurement 1	Measurement 2	Measurement 3	Measurement 4	Measurement 5	Measurement 6	Measurement 7	Measurement 8	Measurement 9	Measurement 10	Mean	s
0.5	7.92	7.93	7.96	7.97	7.96	7.98	7.97	8.00	7.96	7.96	7.96	0.159
0.75	3.66	3.64	3.65	3.66	3.65	3.67	3.64	3.66	3.65	3.64	3.65	0.073
1	2.03	2.04	2.03	2.03	2.04	2.03	2.04	2.03	2.03	2.03	2.04	0.041
1.25	1.31	1.32	1.34	1.32	1.31	1.31	1.31	1.32	1.32	1.32	1.31	0.026
1.5	0.91	0.92	0.91	0.91	0.92	0.91	0.91	0.91	0.91	0.91	0.91	0.018
1.75	0.68	0.68	0.67	0.68	0.69	0.68	0.68	0.68	0.68	0.68	0.68	0.014
2	0.52	0.52	0.52	0.52	0.53	0.53	0.53	0.52	0.52	0.53	0.52	0.010
2.5	0.34	0.34	0.34	0.34	0.34	0.34	0.34	0.34	0.34	0.35	0.34	0.007
3	0.24	0.24	0.23	0.23	0.23	0.23	0.23	0.23	0.24	0.24	0.23	0.005

Table 5 includes the corrected results, mean, and standard deviation (s) for each of the measurement positions. A relative uncertainty of 2% was used to calculate the standard deviation for the Ludlum 9DP measurement means. The relative uncertainty was provided by NIST, as a part of their calibration services. As the Ludlum 9DP is a NIST calibrated secondary standard, these values will be treated as the standard for all other data obtained for this project. These

values were graphed and an equation was fit to the data. The graph, equation fit, and R^2can be found in Figure 2.

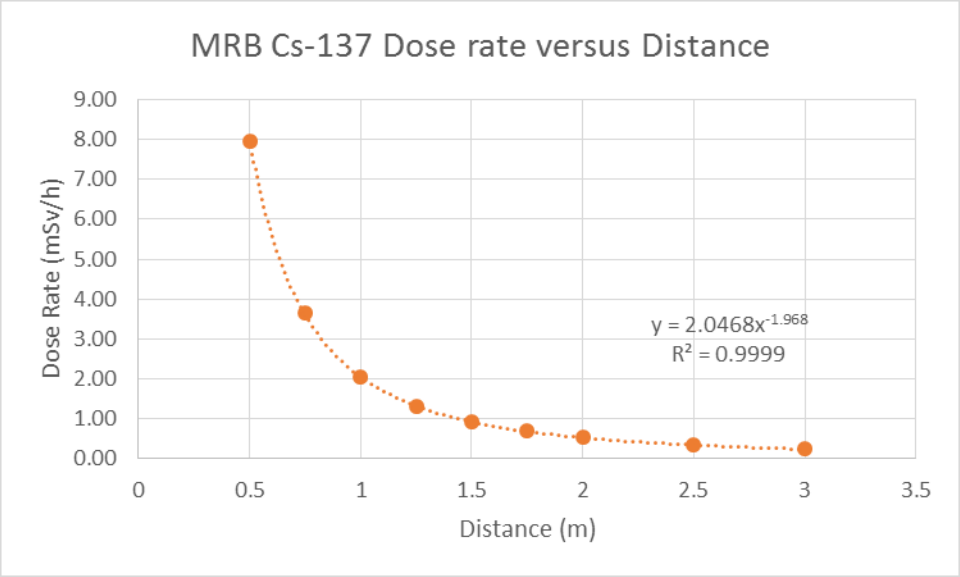

Figure 2. MRB Cs-137 Dose rates versus Distance as measured with the Ludlum 9DP.

MCNP modeling of the MRB Cs-137 source was also completed. The data obtained can be found in Table 6.

Table 6. MRB Cs-137 source characterization results obtained from MCNP

Distance (m)	Gy/photon	Source Activity (Bq)	Photon per Disintegration	Dose Rate (Gy/s)	Dose Rate (Gy/h)	Dose Rate (mSv/h)	Uncertainty
0.5	1.11E-16	23221662500	0.85	2.18E-06	7.86E-03	**7.86**	**0.39**
0.75	5.03E-17	23221662500	0.85	9.93E-07	3.57E-03	**3.57**	**0.18**
1	2.91E-17	23221662500	0.85	5.74E-07	2.07E-03	**2.07**	**0.10**
1.25	1.91E-17	23221662500	0.85	3.76E-07	1.35E-03	**1.35**	**0.07**
1.5	1.35E-17	23221662500	0.85	2.66E-07	9.58E-04	**0.96**	**0.05**
1.75	1.00E-17	23221662500	0.85	1.98E-07	7.13E-04	**0.71**	**0.04**
2	7.77E-18	23221662500	0.85	1.53E-07	5.52E-04	**0.55**	**0.03**
2.5	5.06E-18	23221662500	0.85	9.99E-08	3.60E-04	**0.36**	**0.02**
3	3.58E-18	23221662500	0.85	7.06E-08	2.54E-04	**0.25**	**0.01**

The MCNP output is in Gy/photon, the source activity is the MRB Cs-137 source activity on the date that the Ludlum 9DP calibration measurements were taken, and the relative uncertainty was estimated by the investigators to be 5%. Sources of uncertainty include an uncertainty in the

current source activity of the MRB Cs-137 source, the simplified geometry, and the relative statistical uncertainty provided by the MCNP results. The source activity was calculated by decay correcting the manufacturers assay activity.

Next, a total of 10 measurements at 9 distances from the MRB Cs-137 source were taken using the EPD. The results from these measurements can be found in Table 7.

Table 7. EPD measurement data for the MRB Cs-137 source

EPD MRB Cs-137 30-second measurements units mSv/(hr)												
Distance (M)	Measurement 1	Measurement 2	Measurement 3	Measurement 4	Measurement 5	Measurement 6	Measurement 7	Measurement 8	Measurement 9	Measurement 10	Mean	s
0.5	7.51	7.67	7.49	7.73	7.66	7.78	7.80	7.51	7.55	7.74	7.64	1.529
0.75	3.44	3.44	3.58	3.50	3.55	3.49	3.54	3.56	3.49	3.48	3.51	0.702
1	1.99	2.00	2.02	1.99	1.99	2.02	1.97	2.02	1.96	2.02	2.00	0.399
1.25	1.31	1.28	1.28	1.36	1.27	1.28	1.25	1.25	1.30	1.26	1.28	0.257
1.5	0.92	0.89	0.91	0.90	0.85	0.95	0.90	0.92	0.92	0.92	0.91	0.182
1.75	0.70	0.66	0.65	0.67	0.71	0.67	0.66	0.70	0.62	0.67	0.67	0.134
2	0.53	0.53	0.52	0.55	0.49	0.54	0.49	0.53	0.55	0.49	0.52	0.104
2.5	0.35	0.32	0.31	0.35	0.34	0.34	0.32	0.36	0.32	0.37	0.34	0.068
3	0.22	0.24	0.26	0.23	0.25	0.23	0.20	0.25	0.19	0.23	0.23	0.046

The measurement results, mean, and standard deviation (s) are provided. A relative uncertainty of 20% was used to calculate the standard deviation. The relative uncertainty was provided by the manufacturer of the EPD. These results imply that the EPD does produce results consistent with expectations in a well characterized radiation field produced by a Cs-137 source.

Comparing the means from the MCNP modeling and EPD measurements to the Ludlum 9DP measurements using a t-test, it was determined that the means were statistically similar at the 95% confidence interval for all measurements except one. The only measurement that was found not to be statistically similar to the Ludlum 9DP measurement was the MCNP modeling results for the 3 m position. The calculated t-scores for each measurement can be found in Table 8

Table 8. t-scores for the comparison of means between the MCNP results and EPD results versus the Ludlum 9DP results

Distance (m)	t-score MCNP vs 9DP	t-score EDP vs 9DP
0.5	0.25	0.66
0.75	0.44	0.63
1	0.4	0.32
1.25	0.57	0.377
1.5	0.99	0
1.75	0.75	0.23
2	0.99	0
2.5	0.99	0
3	1.98	0

Rn-222 is a member of the U-238 progeny, as such, it is abundant in areas where local geology contains large amounts of U-238. Rn-222 is a noble gas, has a half-life of 3.82 days, and decays via alpha decay (Johnson, 2017). The Rn-222 progeny includes eleven nuclides and results in either Hg-206 or Pb-206. The decay modes of this progeny include alpha, beta, and gamma emissions. For this project, only the gamma emissions from the Rn-222 progeny and beta emissions from Pb-214 and Bi-214 were considered. This was done as the EPD being tested is used for beta and gamma detection only, and Pb-214 and Bi-214 are the only beta emitters typically found in equilibrium after the Rn-222 decay.

Using the relationship between gamma ray emission and the Bi-214 and Pb-214 beta decay probabilities for the Rn-222 progeny, it is possible to determine the total number of interactions from the Rn-222 progeny gamma rays associated with any measurement via the total number of beta interactions measured. For each Rn-222 decay, there is a certain probability of subsequent radiation emissions from its progeny. These emission probabilities have been well characterized throughout multiple studies (Morel, Etcheverry, & Picolo, 1998). Utilizing the known probabilities, the types of emissions, and the data obtained via MCNP testing, an equation describing the relationship between gamma ray emissions and beta decays has been derived. For all measurements utilizing a two-silicon diode design, a theoretical ratio of the total number of

beta interactions on the unfiltered diode versus the total number of beta interactions on the filtered diode per Rn-222 progeny decay (K_β) can be determined via the following:

$$\mathrm{K_\beta} = \frac{\mathrm{C_u} - \gamma}{\mathrm{C_f} - \gamma \cdot \mathrm{f}}, \tag{17}$$

where c_u is the total number of interactions on the unfiltered diode, c_f is the total number of interactions on the filtered diode, γ is the total number of gamma ray interactions in the unfiltered diode, and f is a correction factor to normalize the total number of gamma ray interactions with the filtered diode. $\mathrm{K_\beta}$ and all associated variables were determined using data obtained via MCNP modeling. Utilizing equation 17 and solving for γ we find:

$$\gamma = \frac{\mathrm{K_\beta} \cdot \mathrm{C_f} - \mathrm{C_u}}{\mathrm{K_\beta} \cdot \mathrm{f} - 1}, \tag{18}$$

where γ is the total number of gamma ray interactions on the unfiltered diode. Using this equation, the total number of beta interactions on an unfiltered diode of an EPD (β_μ) can be calculated by the following:

$$\beta_\mu = \mathrm{C_u} - \gamma \tag{19}$$

where $\mathrm{C_u}$ is the total number of interactions measured on the unfiltered diode of an EPD. In addition to this, the ratio of the total number of gamma ray interactions per Rn-222 progeny decay per the total number of beta interactions per Rn-222 progeny decay ($K_{\gamma/\beta}$) can be determined with the use of the MCNP data. The ratio $K_{\gamma/\beta}$ for the unfiltered diode is given by the following:

$$K_{\gamma/\beta} = \frac{\sigma}{\tau + \omega}, \tag{20}$$

where τ is the total number of interactions in the unfiltered diode per Bi-214 decay, ω is the total number of interactions in the unfiltered diode per Pb-214 decay, and σ is the total number of interactions in the unfiltered diode from gamma rays per Rn-222 progeny decay. Utilizing equations 19 and 20, the total gamma ray contribution as a result of Rn-222 progeny decay on the unfiltered diode of an EPD can be determined via the following:

$$\gamma_{Rn-222} = K_{\gamma/\beta} \cdot \beta_u. \tag{21}$$

The MCNP modeling of the EPD radiation response to Rn-222 and its progeny was completed. The data acquired from MCNP modeling can be found in Table 9.

Table 9. MCNP Rn-222 results for 200,000,000 particles

MCNP Two Diodes 200,000,000 particles	Bi214	Bi214 Prob. Corrected	Pb214	Gamma (Radon Spectrum)
Interactions per starting particle Filtered Diode	0.000019	0.000012	0.000010	0.000201
Interactions per starting particle Unfiltered Diode	0.000175	0.000112	0.000102	0.000210
Total Interactions Per Radon Decay Filtered Diode (C_f)	0.000223			
Total Interactions Per Radon Decay Unfiltered Diode (C_u)	0.000424			
K_β	9.448			
$K_{\gamma/\beta}$	0.985			
Gamma ray correction factor (f)	0.954			
1 m^3 source sampling volume				

Utilizing the results from the MCNP modeling, K_β was determined to be 9.448, $K_{\gamma/\beta}$ was found to be 0.985 $\frac{Rn-222\ \gamma-ray}{Rn-222\ \beta}$, and f was found to be 0.954. K_β and f are both specific to the two diode design utilized for this project. From these results, equation 18 can be rewritten as follows:

$$\gamma = \frac{9.448 \cdot C_f - C_u}{9.01 - 1}. \tag{22}$$

Again, equation 22 is specific to the two diode design utilized in this project. In order to check the validity of equation 22, C_f and C_u from the MCNP results were utilized in the equation and γ was calculated to be the following:

$$\gamma = \frac{9.448 \cdot 0.000223 - 0.000424}{9.01 - 1} \approx 0.000210 \ \frac{\gamma - interactions}{MCNP\ starting\ particle}$$

This result is consistent with the interactions on the unfiltered diode from the Gamma (radon progeny spectrum) MCNP simulation results, which is as expected.

Finally, an MCNP model was run to determine whether alpha particles could contribute to the total number of interactions on the two diode configuration utilized for this project. The maximum alpha energy for Rn-222 progeny of 7.69 MeV was used. A simulation of 200,000,000 particles was run, and zero alpha particles interacted with the either of the diodes. Results indicate that only contributions from beta particles and gamma radiation are measured on the EPD.

Discussion

An EPD, as configured in this research and utilizing the radon discrimination algorithm derived here, can be used by first responders, soldiers, and individuals required to wear personal dosimeters that are not subjected to beta radiation. This system will allow wearers with limited knowledge of radiation safety to complete their work without being confused or distracted by natural radon radiation measurements. As a result, these individuals can maintain their focus on the job at hand.

It is important to clarify that the radon dose discrimination algorithm derived in this research is dependent upon the assumption that the only beta particles detected by the EPD are a result of radon or radon progeny emission. Beta radiation fluence rates at Earth's surface, as a result of cosmic radiation, are not well characterized; however, it is possible that these fluence rates are not negligible. In addition to this, protons and muons associated with cosmic radiation

can contribute to the total number of interactions on the two diodes, which could produce inaccurate results. Because of this, the use of this algorithm may be limited to conditions where cosmic radiation is shielded. These conditions would include being inside of a building or vehicle, underground, or under water. Exposure to unshielded sources of beta radiation would also negatively affect the results of this algorithm; however, a scenario in which a first responder would be exposed to an unshielded beta source without prior knowledge of the source's existence is very unlikely.

While the results for K_β and equation 22 are specific to the two diode configuration utilized in this research, these values can easily be determined for any two diode configuration. Using MCNP, any two diode configuration can be modeled and the steps presented in this research can be followed to determine K_β specific to that configuration.

In order to utilize the radon dose discrimination algorithm derived in this research, the raw data for the total number of ionizing radiation particles that interact with the diodes must be used. If the data have been energy compensated or manipulated in any other way, the results may not be accurate.

An additional test was conducted to determine the validity of the results presented in this thesis. MCNP was used to simulate a gamma radiation source in the presence of radon. Using the data from this simulation, C_f and C_u were constructed and γ was determined. Utilizing γ, β_u, and γ_{Rn-222} were calculated. The calculated value for γ_{Rn-222} was then compared to the MCNP results and was determined to be consistent with the MCNP output. This test confirms that the gamma radiation contribution from radon and its progeny can be discriminated from the gamma radiation contribution from other sources utilizing the algorithm derived in this research.

CHAPTER 4 CONCLUSION

The MRB Cs-137 calibration was completed and a dose rate equation was found to be the following:

$$\dot{D}(x) = \frac{2.0468}{x^{1.968}}, \tag{23}$$

where $\dot{D}$ is the dose rate in mSv/h, and x is the distance from the source along the centerline of the beam. This equation can be utilized to conduct device calibration with the MRB Cs-137 source.

The EPD and MCNP modeling produced statistically consistent results with the Ludlum 9DP ion chamber. The results of this study suggest that the EPD can produce reliable results in a fixed energy gamma radiation field; however, further testing is required to determine the EPDs ability to produce reliable results in mixed radiation fields.

Finally, an equation to determine the total Rn-222 progeny's gamma radiation contribution for a two diode EPD was derived and tested. The testing conducted confirms that equation 18 produces results consistent with expectations. Utilizing equation 18, it is possible to discriminate Rn-222 progeny contributions to the exposure measurements of first responders equipped with an EPD operating a two diode configuration as modeled in this project. After the Rn-222 progeny contribution is removed, it is possible to determine whether a first responder is exposed to a non-background source of ionizing radiation, when the background contribution from cosmic radiation is known and subtracted from the results. Also, equation 10 can be utilized for any two diode EPD, when equation 17 is utilized to determine a value for K_β that is specific to that two diode configuration.

REFERENCES

American Association of Physicists in Medicine. (2012, June 1). *09b AAPM Report NO. 181 - Calibrators.* Retrieved from United States Nuclear Regulatory Commission: https://www.nrc.gov/docs/ML1226/ML12261A350.pdf

ICRP. (2008). *Nuclear Decay Data for Dosimetric Calculations.* ICRP Publication 107 .

ICRP. (2012). *Copendium of Dose Coeffecients Based on ICRP Publication 60.* ICRP Publication.

Johnson, T. E. (2017). *Introduction to Health Physics.* New York: Mcgraw-Hill Education.

Knight, R., & Jones, B. (2010). *College Physics.* Glenview: Addison-Wesley.

Knoll, G. F. (2010). *Radiation Detection and Measurement.* Ann Arbor : John Wiley & Sons, INC.

Lee, W., Lee, B. J., & Lee, C. W. (2003). Develovpement of Personal Dosimter Using Electronic Conversion Method. *Proceedings of the Korean Nuclear Spring Meeting.* Gyeong Ju.

Los Alamos National Labratory. (2018, Dec. 5). *A General Monte Carlo N-Particle (MCNP) Transport Code.* Retrieved from Los Alamos National Labratory: https://mcnp.lanl.gov/

Ludlum Measurements, INC. (2018, December). *Ludlum Model 9DP.* Retrieved from Ludlum Measurements, INC.: https://ludlums.com/images/product_manuals/M9DP_&_M9DPstar.pdf

Mitra, P., Srivastava, S., Singh, S. K., Akar, D. K., Patni, H. k., Topkar, A., & Kumar, A. V. (2016). Optimum Energy Compensation for Current Mode Application of Silicon PIN Diode Gamma Radiation Detection. *IEEE Transactions on Nuclear Science, Vol. 63, NO. 6, December 2016*.

Morel, J., Etcheverry, M., & Picolo, J. (1998). Main gamma-rays emission probabilities of radon-222 daughters. *Bulletin du Bureau National de Metrologie*, 15-20.

National Council on Radiation Protection and Measurements. (1991). *NCRP Report No. 112.* Bethesda: National Council on Radiation Protection and Measurements.

NIST. (2019, 3 25). *Two-Sample t-Test for Equal Means*. Retrieved from Engineering Statistics Handbook: https://www.itl.nist.gov/div898/handbook/eda/section3/eda353.htm

Omar, A. (2010). *Silicon Diode Dose Response Corrections in Small Photon Feilds.* Stockholm: Stockholm University.

APPENDIX

Bi-214 and Pb-214 Probabilities

Bi-214	125	P	Pb-214	111	P
0	8.97E-01	0.00E+00	0	3.02E+00	0.00E+00
0.0001	8.97E-01	8.97E-05	0.0001	3.02E+00	3.02E-04
0.00011	8.97E-01	8.97E-06	0.00011	3.02E+00	3.02E-05
0.00012	8.97E-01	8.97E-06	0.00012	3.02E+00	3.02E-05
0.00013	8.97E-01	8.97E-06	0.00013	3.02E+00	3.02E-05
0.00014	8.97E-01	8.97E-06	0.00014	3.02E+00	3.02E-05
0.00015	8.97E-01	8.97E-06	0.00015	3.02E+00	3.02E-05
0.00016	8.97E-01	8.97E-06	0.00016	3.02E+00	3.02E-05
0.00018	8.97E-01	1.79E-05	0.00018	3.02E+00	6.04E-05
0.0002	8.97E-01	1.79E-05	0.0002	3.02E+00	6.04E-05
0.00022	8.97E-01	1.79E-05	0.00022	3.02E+00	6.04E-05
0.00024	8.97E-01	1.79E-05	0.00024	3.02E+00	6.04E-05
0.00026	8.97E-01	1.79E-05	0.00026	3.02E+00	6.04E-05
0.00028	8.97E-01	1.79E-05	0.00028	3.02E+00	6.04E-05
0.0003	8.97E-01	1.79E-05	0.0003	3.02E+00	6.04E-05
0.00032	8.97E-01	1.79E-05	0.00032	3.02E+00	6.04E-05
0.00036	8.97E-01	3.59E-05	0.00036	3.02E+00	1.21E-04
0.0004	8.97E-01	3.59E-05	0.0004	3.02E+00	1.21E-04
0.00045	8.97E-01	4.48E-05	0.00045	3.02E+00	1.51E-04
0.0005	8.97E-01	4.48E-05	0.0005	3.02E+00	1.51E-04
0.00055	8.97E-01	4.48E-05	0.00055	3.02E+00	1.51E-04
0.0006	8.97E-01	4.48E-05	0.0006	3.02E+00	1.51E-04
0.00065	8.97E-01	4.48E-05	0.00065	3.02E+00	1.51E-04

0.0007	8.97E-01	4.48E-05	0.0007	3.02E+00	1.51E-04
0.00075	8.97E-01	4.48E-05	0.00075	3.02E+00	1.51E-04
0.0008	8.97E-01	4.48E-05	0.0008	3.02E+00	1.51E-04
0.00085	8.97E-01	4.48E-05	0.00085	3.02E+00	1.51E-04
0.0009	8.97E-01	4.48E-05	0.0009	3.02E+00	1.51E-04
0.001	8.97E-01	8.97E-05	0.001	3.02E+00	3.02E-04
0.0011	8.97E-01	8.97E-05	0.0011	3.02E+00	3.02E-04
0.0012	8.97E-01	8.97E-05	0.0012	3.02E+00	3.02E-04
0.0013	8.97E-01	8.97E-05	0.0013	3.02E+00	3.02E-04
0.0014	8.97E-01	8.97E-05	0.0014	3.01E+00	3.02E-04
0.0015	8.97E-01	8.97E-05	0.0015	3.01E+00	3.01E-04
0.0016	8.97E-01	8.97E-05	0.0016	3.01E+00	3.01E-04
0.0018	8.97E-01	1.79E-04	0.0018	3.01E+00	6.03E-04
0.002	8.97E-01	1.79E-04	0.002	3.01E+00	6.02E-04
0.0022	8.97E-01	1.79E-04	0.0022	3.01E+00	6.02E-04
0.0024	8.97E-01	1.79E-04	0.0024	3.01E+00	6.02E-04
0.0026	8.97E-01	1.79E-04	0.0026	3.01E+00	6.02E-04
0.0028	8.97E-01	1.79E-04	0.0028	3.01E+00	6.01E-04
0.003	8.97E-01	1.79E-04	0.003	3.01E+00	6.01E-04
0.0032	8.97E-01	1.79E-04	0.0032	3.00E+00	6.01E-04
0.0036	8.97E-01	3.59E-04	0.0036	3.00E+00	1.20E-03
0.004	8.97E-01	3.59E-04	0.004	3.00E+00	1.20E-03
0.0045	8.98E-01	4.49E-04	0.0045	3.00E+00	1.50E-03
0.005	8.98E-01	4.49E-04	0.005	2.99E+00	1.50E-03
0.0055	8.98E-01	4.49E-04	0.0055	2.99E+00	1.50E-03
0.006	8.98E-01	4.49E-04	0.006	2.99E+00	1.50E-03
0.0065	8.98E-01	4.49E-04	0.0065	2.98E+00	1.49E-03
0.007	8.98E-01	4.49E-04	0.007	2.98E+00	1.49E-03

0.0075	8.98E-01	4.49E-04	0.0075	2.98E+00	1.49E-03
0.008	8.98E-01	4.49E-04	0.008	2.98E+00	1.49E-03
0.0085	8.98E-01	4.49E-04	0.0085	2.97E+00	1.49E-03
0.009	8.98E-01	4.49E-04	0.009	2.97E+00	1.49E-03
0.01	8.98E-01	8.98E-04	0.01	2.96E+00	2.97E-03
0.011	8.98E-01	8.98E-04	0.011	2.96E+00	2.96E-03
0.012	8.98E-01	8.98E-04	0.012	2.95E+00	2.96E-03
0.013	8.99E-01	8.98E-04	0.013	2.95E+00	2.95E-03
0.014	8.99E-01	8.99E-04	0.014	2.94E+00	2.95E-03
0.015	8.99E-01	8.99E-04	0.015	2.93E+00	2.94E-03
0.016	8.99E-01	8.99E-04	0.016	2.93E+00	2.93E-03
0.018	9.01E-01	1.80E-03	0.018	2.92E+00	5.85E-03
0.02	9.03E-01	1.80E-03	0.02	2.92E+00	5.85E-03
0.022	9.05E-01	1.81E-03	0.022	2.91E+00	5.83E-03
0.024	9.07E-01	1.81E-03	0.024	2.90E+00	5.82E-03
0.026	9.08E-01	1.81E-03	0.026	2.90E+00	5.80E-03
0.028	9.10E-01	1.82E-03	0.028	2.89E+00	5.79E-03
0.03	9.12E-01	1.82E-03	0.03	2.88E+00	5.78E-03
0.032	9.14E-01	1.82E-03	0.032	2.87E+00	5.76E-03
0.036	9.17E-01	3.65E-03	0.036	2.86E+00	1.15E-02
0.04	9.20E-01	3.67E-03	0.04	2.85E+00	1.14E-02
0.045	9.24E-01	4.60E-03	0.045	2.83E+00	1.42E-02
0.05	9.28E-01	4.62E-03	0.05	2.81E+00	1.41E-02
0.055	9.32E-01	4.64E-03	0.055	2.79E+00	1.40E-02
0.06	9.36E-01	4.66E-03	0.06	2.77E+00	1.39E-02
0.065	9.39E-01	4.68E-03	0.065	2.75E+00	1.38E-02
0.07	9.43E-01	4.70E-03	0.07	2.72E+00	1.37E-02
0.075	9.46E-01	4.71E-03	0.075	2.70E+00	1.36E-02

0.08	9.49E-01	4.73E-03	0.08	2.68E+00	1.35E-02
0.085	9.52E-01	4.75E-03	0.085	2.66E+00	1.34E-02
0.09	9.55E-01	4.76E-03	0.09	2.64E+00	1.33E-02
0.1	9.61E-01	9.55E-03	0.1	2.59E+00	2.64E-02
0.11	9.66E-01	9.61E-03	0.11	2.55E+00	2.59E-02
0.12	9.71E-01	9.66E-03	0.12	2.51E+00	2.55E-02
0.13	9.76E-01	9.71E-03	0.13	2.46E+00	2.51E-02
0.14	9.80E-01	9.76E-03	0.14	2.42E+00	2.46E-02
0.15	9.83E-01	9.80E-03	0.15	2.37E+00	2.42E-02
0.16	9.86E-01	9.83E-03	0.16	2.33E+00	2.37E-02
0.18	9.92E-01	1.97E-02	0.18	2.25E+00	4.66E-02
0.2	9.96E-01	1.98E-02	0.2	2.18E+00	4.50E-02
0.22	9.98E-01	1.99E-02	0.22	2.09E+00	4.35E-02
0.24	9.99E-01	2.00E-02	0.24	2.00E+00	4.18E-02
0.26	9.98E-01	2.00E-02	0.26	1.91E+00	4.01E-02
0.28	9.97E-01	2.00E-02	0.28	1.81E+00	3.82E-02
0.3	9.93E-01	1.99E-02	0.3	1.71E+00	3.62E-02
0.32	9.89E-01	1.99E-02	0.32	1.60E+00	3.41E-02
0.36	9.75E-01	3.95E-02	0.36	1.38E+00	6.40E-02
0.4	9.57E-01	3.90E-02	0.4	1.16E+00	5.52E-02
0.45	9.28E-01	4.78E-02	0.45	8.80E-01	5.78E-02
0.5	8.93E-01	4.64E-02	0.5	6.21E-01	4.40E-02
0.55	8.54E-01	4.46E-02	0.55	3.94E-01	3.11E-02
0.6	8.10E-01	4.27E-02	0.6	2.12E-01	1.97E-02
0.65	7.63E-01	4.05E-02	0.65	9.21E-02	1.06E-02
0.7	7.14E-01	3.82E-02	0.7	4.16E-02	4.61E-03
0.75	6.63E-01	3.57E-02	0.75	2.72E-02	2.08E-03
0.8	6.12E-01	3.31E-02	0.8	1.93E-02	1.36E-03

0.85	5.61E-01	3.06E-02
0.9	5.10E-01	2.80E-02
1	4.11E-01	5.10E-02
1.1	3.23E-01	4.11E-02
1.2	2.48E-01	3.23E-02
1.3	1.86E-01	2.48E-02
1.4	1.39E-01	1.86E-02
1.5	1.12E-01	1.39E-02
1.6	9.82E-02	1.12E-02
1.8	7.80E-02	1.96E-02
2	6.40E-02	1.56E-02
2.2	4.99E-02	1.28E-02
2.4	3.59E-02	9.98E-03
2.6	2.30E-02	7.17E-03
2.8	1.24E-02	4.60E-03
3	4.46E-03	2.48E-03
3.2	3.38E-04	8.93E-04
3.272	0.00E+00	2.43E-05

0.85	1.23E-02	9.62E-04
0.9	6.55E-03	6.14E-04
1	2.54E-04	6.55E-04
1.023	0.00E+00	5.85E-06